Applications of the Finite Area Method on a Geographic Scale: From Dense Snow Avalanches to Turbidity Currents

Matthias Rauter[123], Kate Heerema[4], Dieter Issler[1], Peter Talling[4]

1) Department of Natural Hazards, Norwegian Geotechnical Institute, Oslo, Norway
2) Department of Mathematics, University of Oslo, Oslo, Norway
3) Unit of Geotechnical and Tunnel Engineering, University of Innsbruck, Innsbruck, Austria
4) Departments of Geography and Earth Sciences, University of Durham, United Kingdom

Corresponding author: matthias.rauter@ngi.no,
Sognsv. 72, 0855 Oslo
+43 650 4205640

1. Introduction

Gravitational mass flows (GMF), such as snow avalanches, debris flows, landslides, lahars, pyroclastic density currents and turbidity currents are natural hazards with high socio-economic impact. For instance, the annual damages of landslides in alpine countries is estimated as USD 1-5 billion (Kjekstad and Highland, 2009). Pyroclastic density currents are responsible for more than 50% of global volcanic fatalities (Lube et al., 2019). Even turbidity currents, often undervalued and overlooked, have far-reaching consequences as they are capable of severely damaging seafloor infrastructure (Heezen and Ewing, 1952). These include telecommunication cables that form the backbone of the internet, and carry 95% of all global data traffic (Carter et al., 2014).

Despite their importance to the general community, GMFs are relatively poorly understood. These violent flows are notoriously difficult to measure directly in the field, as they are often powerful enough to damage the measurement instruments (Lube et al., 2019; Inman, 1976; Gauer et al., 2007). The natural hazard community has therefore depended on numerical models to deepen our understanding of processes, to evaluate and explain past events, and to predict and manage future events and risks.

Gravitational mass flows comprise a wide spectrum of phenomena where gravity transports a mixture of grains (sediment or other) and fluid (water or air) down a slope. With regard to the dominant stress transmission mechanism, one end of the spectrum is represented by dense granular flows, such as landslides and dense snow avalanches, where grain-to-grain collisions are the major mechanical forces. The other end of the spectrum are dilute suspended particle flows, e.g. powder snow avalanches, turbidity currents and pyroclastic density currents, where turbulent stresses transfer momentum. Debris flows are an intermediate stage, where dense fluid-grain-mixtures create a strong, cohesive, matrix-supported flow. This wide variety of grain suspension mechanisms makes numerical modeling challenging, and no generally applicable model has been found so far. However, a large variety of models has been developed, focusing on one of the mentioned transport mechanisms. Most notable and

relevant for this work are the developments of Eglit, Grigorian and co-workers (e.g. Eglit, 1967) and Savage and Hutter (1989), focusing on dense granular flows (e.g. dense snow avalanches, see Figure 1), and Parker et al. (1986), focusing on turbidity currents (see Figure 2).

Figure 1: A dense snow avalanche, released from a failing snowpack. The avalanche travels as a relatively dense flow downhill. The dense flow is sometimes accompanied by a dilute powder cloud. In here we focus on the dense core, which is usually the most destructive part of the avalanche. Photo: J. Schweizer, SLF.
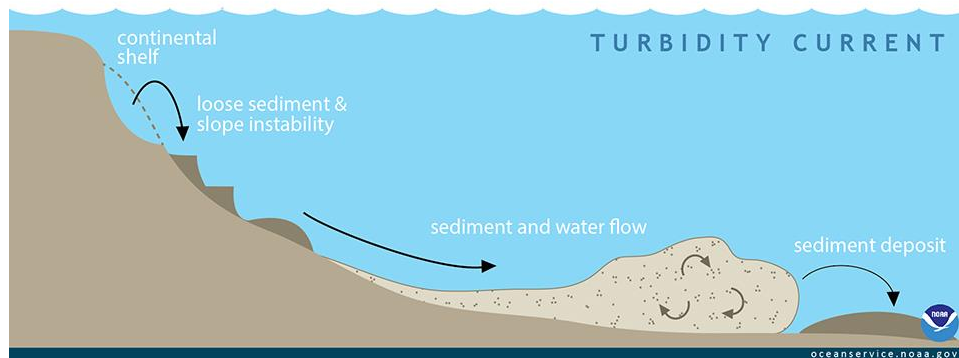

Figure 2: Sketch of a turbidity current. Increased density due to suspended sediment initiates downslope movement and further entrainment of sediment. Sketch: NOAA.

The dense granular flow (Savage and Hutter, 1989) and turbidity current (Parker et al., 1986) models are based on depth-integrated conservation laws, similar to the shallow water equations. Depth-integration reduces the computational cost dramatically, making real case applications possible. Still, these models are numerically challenging and solutions were initially limited to one-dimensional cases and simple geometries. Full numerical solutions of gravitational mass flows in complex terrain started to emerge in the 1990s. The Finite Area Method (Tuković and Jasak, 2012), as recently introduced in OpenFOAM

(v1712 and upwards), provides a convenient framework for the implementation of arbitrary depth-integrated GMF models (Rauter and Tuković, 2018). The interaction with complex terrain is handled by the Finite Area framework and the solver code is reduced to physical processes, i.e. the transport equations, rheology, and entrainment. We will present two depth-integrated GMF models, as implemented into OpenFOAM-v1812, and their application to real cases. Extensive data for both models is available for comparison and validation, creating an outstanding opportunity to compare numerical modeling efforts with direct measurements.

The first model is based on the Savage-Hutter equations (Savage and Hutter, 1989) and aims to simulate snow avalanches (see Figure 1). It includes dry friction and entrainment of additional snow at the base. Dry friction is proportional to the basal pressure, which is determined through the momentum balance normal to the surface. We will show its capabilities by simulating a catastrophic dense snow avalanche (Rauter et al., 2018).

The second model is based on the work of Parker et al. (1986) for turbidity currents. The solver models a turbulent mixture of sediment and water, including entrainment of sediment at the bottom and water at the top. It will be applied to a turbidity current in Monterey Canyon, off the coast of California.

2. Method

A shallow flow can be expressed as a two-dimensional mathematical problem by integrating the respective conservation equations. This results in partial differential equations, expressed in terms of gradients along the surface, over which the flow travels. The Finite Area Method provides all operators that are required for this class of models. This allows for relatively straight-forward implementation of shallow GMF models, by assembling the respective terms with the OpenFOAM programming interface (API) (OpenCFD, 2018). We will denote gradients along the surface with $\boldsymbol{\nabla}$, surface tangential components with index s, and surface normal components with an index n in the following (for details see Rauter and Tuković, 2018).

2.1 Savage-Hutter model

The solver *faSavageHutterFoam* follows the general assumptions of Savage and Hutter (1989) and describes the flow thickness h and depth-averaged velocity $\overline{\boldsymbol{u}}$ of a granular flow with density ρ on complex terrain,

$$\frac{\partial h}{\partial t} + \boldsymbol{\nabla} \cdot (h\overline{\boldsymbol{u}}) = e^{(s)},$$

$$\frac{\partial h\overline{\boldsymbol{u}}}{\partial t} + \boldsymbol{\nabla}_s \cdot (h\overline{\boldsymbol{u}\boldsymbol{u}}) = -\frac{1}{\rho}\boldsymbol{\tau}_b + h\boldsymbol{g}_s - \frac{1}{2\rho}\boldsymbol{\nabla}_s(hp_b),$$

$$\boldsymbol{\nabla}_n \cdot (h\overline{\boldsymbol{u}\boldsymbol{u}}) = h\boldsymbol{g}_n - \frac{1}{2\rho}\boldsymbol{\nabla}_n(hp_b) - \frac{1}{\rho}\boldsymbol{n}_b p_b.$$

The first equation represents the conservation of mass, the second equation the conservation of surface tangential momentum and the third equation the surface normal momentum balance. $\boldsymbol{g_s}$ is the surface tangential gravitational acceleration and $\boldsymbol{g_n}$ the surface normal gravitational acceleration, $\boldsymbol{n_b}$ is the surface normal. The volumetric entrainment rate of snow $e^{(s)}$ and basal friction $\boldsymbol{\tau_b}$ are expressed as local functions of the depth-integrated velocity $\overline{\boldsymbol{u}}$ and basal pressure p_b (for details see Rauter et al., 2018 and Savage and Hutter, 1989).

2.2 Parker-Fukushima model

The solver *faParkerFukushimaFoam* implements the turbulent four equation model of Parker et al. (1986). It can be written in terms of flow thickness h, depth-averaged velocity $\overline{\boldsymbol{u}}$, volumetric sediment concentration c, and turbulent kinetic energy k,

$$\frac{\partial h}{\partial t} + \boldsymbol{\nabla} \cdot (h\overline{\boldsymbol{u}}) = e^{(w)},$$

$$\frac{\partial h\overline{\boldsymbol{u}}}{\partial t} + \boldsymbol{\nabla_s} \cdot (h\overline{\boldsymbol{u}\boldsymbol{u}}) = rch\boldsymbol{g_s} - \frac{1}{2}r\boldsymbol{\nabla_s}(ch^2|\boldsymbol{g_n}|) - u_*^2\frac{\overline{\boldsymbol{u}}}{|\overline{\boldsymbol{u}}|},$$

$$\frac{\partial ch}{\partial t} + \boldsymbol{\nabla} \cdot (ch\overline{\boldsymbol{u}}) = e^{(s)} - d^{(s)},$$

$$\frac{\partial kh}{\partial t} + \boldsymbol{\nabla} \cdot (kh\overline{\boldsymbol{u}}) = u_*^2|\overline{\boldsymbol{u}}| + \frac{1}{2}|\overline{\boldsymbol{u}}|^3 e^{(w)} - \epsilon_0 h - rch\mathrm{g}v^{(s)} - \frac{1}{2}rgch|\overline{\boldsymbol{u}}|e^{(w)} - \frac{1}{2}rgh\big(e^{(s)} - d^{(s)}\big).$$

The equations represent the balances of water, tangential momentum, suspended sediment, and turbulent kinetic energy. The suspended sediment has a weight ratio $r = \big(\rho^{(s)} - \rho^{(w)}\big)/\rho^{(w)}$. $e^{(w)}$ and $e^{(s)}$ represent the entrainment rate of water and sediment respectively, $d^{(s)}$ the deposition rate of sediment, u_*^2 the turbulent wall friction, and $v^{(s)}$ the settling velocity of the sediment. All of these variables are modeled as functions of local flow fields (for details, see Parker et al., 1986).

2.3 Pre- and Post-processing

Pre- and post-processing are mainly conducted via a Geographic Information System (GIS), i.e. QGIS. GIS data is translated to OpenFOAM dictionaries using python scripts. This enables the user to enter terrain or bathymetry data, simulation borders, areas for mesh refinement, and initial conditions in a user-friendly interface. OpenFOAM results can be exported to GIS data format in a similar manner, allowing post-processing and inclusion in respective databases.

The Finite Area Method operates on the boundary mesh of a Finite Volume mesh. A mesh is generated that covers the volume above the terrain of interest; but only the bottom boundary mesh is utilized. cfMesh (*pMesh*) is applied in polygon-dominated mode with aggressive refinements near relevant surfaces for mesh-generation (see Figure 3). cfMesh is able to create smooth surface meshes of high

quality, which is necessary for the stability of the Finite Area Method. This is a significant outcome, considering the irregular topography of mountainous terrain and submarine canyons.

The snow avalanche is initiated by a sudden release of the entire snow pack in an unstable region (release area). The turbidity current is initiated by an inlet flow, where a Dirichlet (fixedValue) boundary condition is set. The rest of the boundaries are specified as Neumann (zeroGradient) boundary conditions. Further details on the simulation setup can be found in Rauter et al., 2018.

Figure 3: Surface mesh of Monterey submarine canyon as generated by cfMesh (pMesh). The Finite Area Method operates on the boundary of a normal Finite Volume Mesh and all Finite Volume meshers can be applied (for details see Rauter et al., 2018).

3. Results and Discussion

3.1 Wolfsgruben Dense Snow Avalanche

The following results show a back-calculation of the Wolfsgruben avalanche from 13 March 1988. The avalanche struck inhabited areas and is therefore well studied and documented.

Figure 4 shows the timeline of the avalanche simulation. The snowpack with a thickness of approximately 1.5m is released at t=0s and travels downslope with a velocity of up to 50 m/s. It reaches the village at t=60s and comes to rest at t=80s with a deposition thickness of up to 12m. Figure 5, left, highlights the export to GIS and figure 5, right, shows further processing in GIS to incorporate geographic data such as orthophotos, basemaps and historic records.

A comparison of the simulated avalanche with the documented deposit (Figure 5, right) shows a satisfying model performance within expected uncertainty of depth-integrated GMF models. Errors can be mainly attributed to model assumptions and terrain data quality. Furthermore, the comparison to a commercial avalanche simulation software showed good agreement (Rauter et al., 2018).
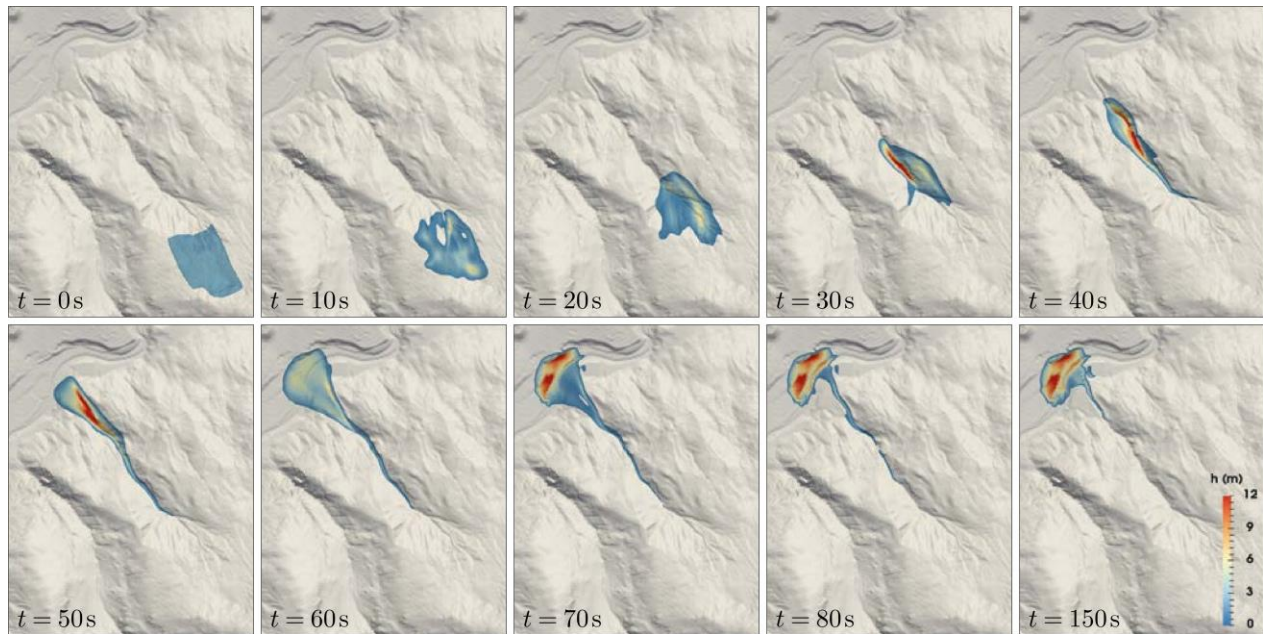
Figure 4: Time series of the Wolfsgruben avalanche as simulated with faSavageHutterFoam and visualized in ParaView. The color scale represents flow thickness, which is clipped at 0.5m.
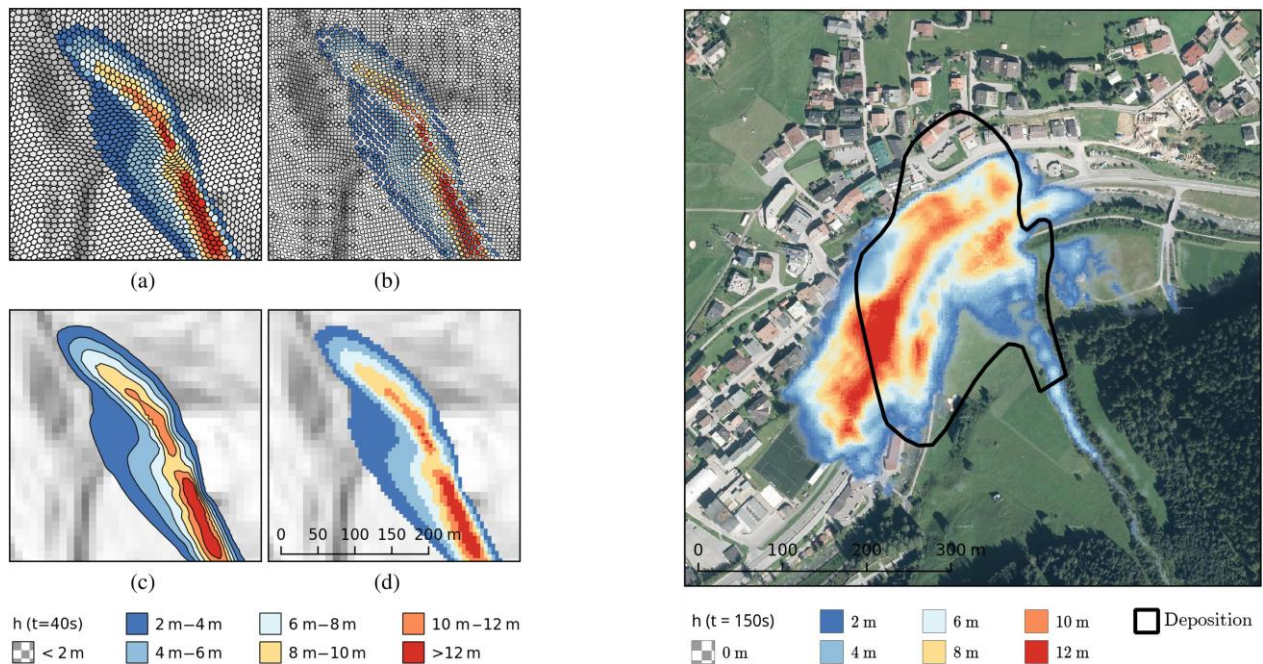

Figure 5: Left: The flow thickness field _h_ at time t=40s. The figure shows four methods to export and analyze results in GIS: export of cells as polygons (a); export of cell centers as points (b); export of contour lines as polygons (c); remapping of the unstructured FA mesh to a regular raster (d). Right: Deposition (i.e. flow thickness after still stand) in QGIS alongside an orthophoto of the relevant area showing affected houses and infrastructure. The black line marks the outline of the 1988 deposition.

t=4000s t=5500s t=7000s

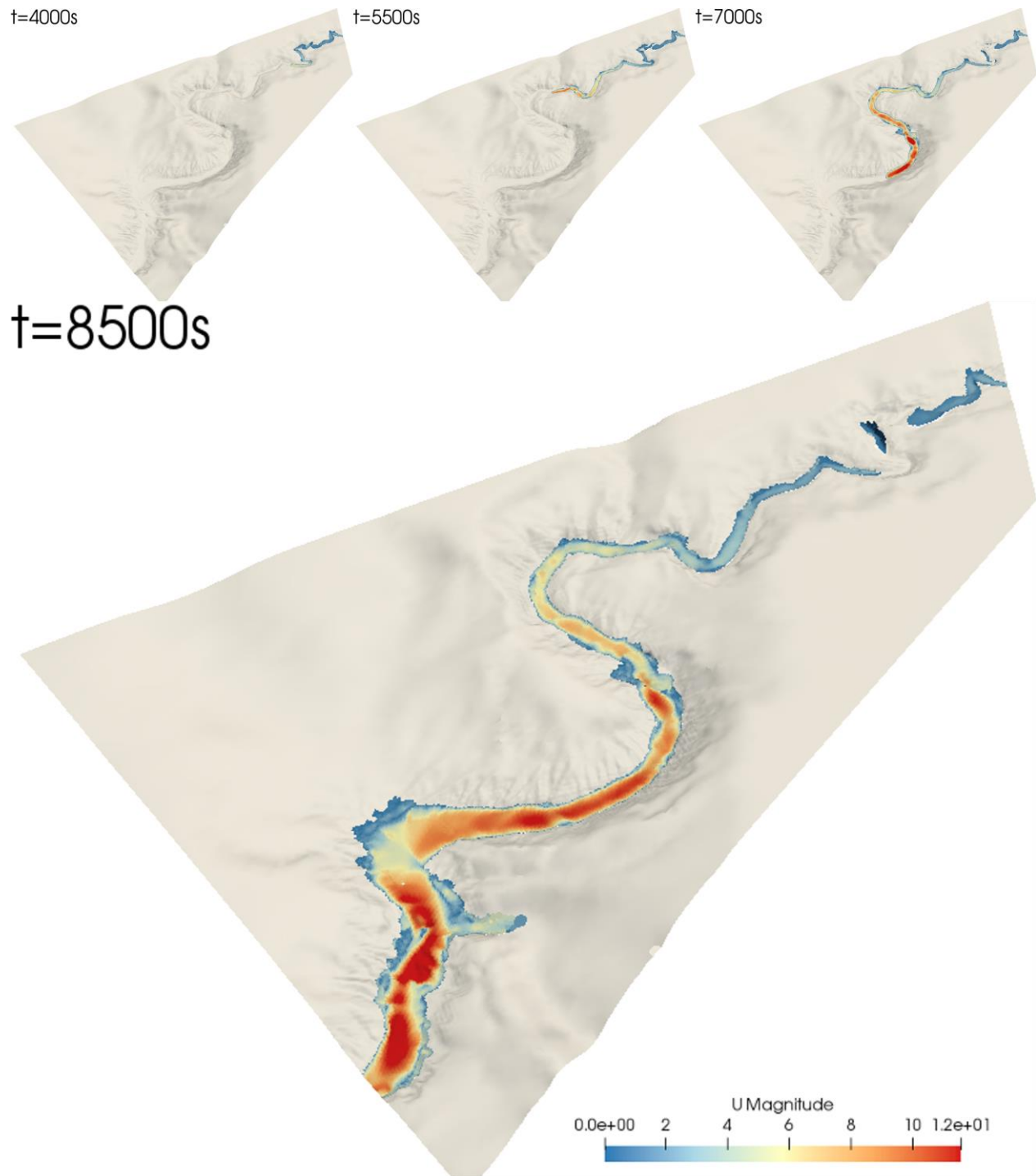t=8500s

U Magnitude

0.0e+00 2 4 6 8 10 1.2e+01

Figure 6: Numerical simulation of a turbidity current in the Monterey Canyon with faParkerFukushimaFoam. The inlet (right side of simulation domain) is positioned at a monitoring station and input is chosen to match respective data. The turbidity current entrains large amounts of bed sediment in the simulation and accelerates substantially.

3.2 Monterey Canyon Turbidity Current

Monterey Canyon has been extensively monitored in recent years, and a high frequency of annual turbidity currents was found in the upper canyon. The latest, 18-month, monitoring study (Paull et al., 2018) resulted in new insights into these mass movements, which usually remain hidden underneath the sea surface. A large array of monitoring stations provides unprecedented information about flow velocities and flow thickness along the canyon. We use the first monitoring station as input data for the inlet. All following monitoring stations are used for validation.

Figure 6 shows the timeline of the numerical simulation with faParkerFukushimaFoam. The turbidity current enters the simulation domain at the right side with modest velocity and sediment concentration. The velocity in this example is sufficient to entrain large amounts of bed sediment, increasing the density of the flow, which leads to further acceleration; the turbidity current ignites and becomes a violent and destructive flow.

4 Conclusion and Summary

Gravitational mass flows are as diverse as they are common. The large diversity of physical processes involved in GMFs requires easily adaptable solvers. The Finite Area framework fulfills these requirements, as we have demonstrated by modeling two distinctly different gravitational mass flows.

The two solvers, *faSavageHutterFoam* for dense snow avalanches and *faParkerFukushimaFoam* for turbidity currents, implement distinctly different flow models, represented by their solver code. The models perform satisfactorily, considering the simplifications involved in the mathematical modeling of such flows and the uncertainty of the initial or boundary conditions. The avalanche solver has been evaluated thoroughly (Rauter et al., 2018), and future efforts are veered towards verifying and evaluating the turbidity current model. What makes the Finite Area Method special is the application of a three-dimensional surface mesh, which enables simple handling of complex terrain. Encapsulating the handling of complex topography in the Finite Area framework simplifies and accelerates model development and makes OpenFOAM and the Finite Area Method an appealing tool for modeling GMFs. However, the generation of a 3D mesh is complicated, computationally expensive and might represent a hurdle for inexperienced users.

The small family of Finite Area solvers that we have developed provide the ideal platform for testing new modeling approaches and for bringing them into operation quickly. The rapid implementation of numerical approaches allows for easy integration of new insights from field datasets, new theories, and laboratory models. Combining these methodologies will improve our understanding of these natural hazards and help mitigate them in the future.

References:

Carter, L., Gavey, R., Talling, P. J., & Liu, J. T. (2014). Insights into submarine geohazards from breaks in subsea telecommunication cables. Oceanography, 27(2), 58-67.

Eglit, M. E. (1967). Teoreticheskie podkhody k raschetu dvizheniia snezhnyk lavin. (Theoretical approaches to avalanche dynamics). Itogi Nauki Gidrol. Sushi. Gliatsiol. English translation in: Soviet Avalanche Research – Avalanche Bibliography Update: 1977–1983. Glaciological Data Report GD-16, pages 63–116. World Data Center A for Glaciology [Snow and Ice], 1984, pp. 69–97.

Gauer, P., Kern, M., Kristensen, K., Lied, K., Rammer, L., & Schreiber, H. (2007). On pulsed Doppler radar measurements of avalanches and their implication to avalanche dynamics. Cold Regions Science and Technology, 50(1-3), 55-71.

Heezen, B. C., & Ewing, W. M. (1952). Turbidity currents and submarine slumps, and the 1929 Grand Banks [Newfoundland] earthquake. American journal of Science, 250(12), 849-873.

Inman, D. L., Nordstrom, C. E., & Flick, R. E. (1976). Currents in submarine canyons: An air-sea-land interaction. Annual Review of Fluid Mechanics, 8(1), 275-310.

Kjekstad, O., & Highland, L. (2009). Economic and social impacts of landslides. In Landslides–disaster risk reduction (pp. 573-587). Edited by Sassa, K. and Canuti, P. Springer, Berlin, Heidelberg.

Lube, G., Breard, E. C., Jones, J., Fullard, L., Dufek, J., Cronin, S. J., & Wang, T. (2019). Generation of air lubrication within pyroclastic density currents. Nature Geoscience, 12(5), 381.

OpenCFD Ltd.: OpenFOAM – The Open Source CFD Toolbox – User Guide, available at: https://www.openfoam.com/documentation/user-guide/ (last access: 31 January 2018), 2004.

Parker, G., Fukushima, Y., & Pantin, H. M. (1986). Self-accelerating turbidity currents. Journal of Fluid Mechanics, 171, 145-181.

Paull, C. K., Talling, P. J., Maier, K. L., Parsons, D., Xu, J., Caress, D. W., ... & Chaffey, M. (2018). Powerful turbidity currents driven by dense basal layers. Nature communications, 9(1), 4114.

Rauter, M., Kofler, A., Huber, A., & Fellin, W. (2018). faSavageHutterFOAM 1.0: depth-integrated simulation of dense snow avalanches on natural terrain with OpenFOAM. Geoscientific Model Development, 11(7), 2923-2939.

Rauter, M., & Tuković, Ž. (2018). A finite area scheme for shallow granular flows on three-dimensional surfaces. Computers & Fluids, 166, 184-199.

Savage, S. B., & Hutter, K. (1989). The motion of a finite mass of granular material down a rough incline. Journal of fluid mechanics, 199, 177-215.

Tuković, Ž., & Jasak, H. (2012). A moving mesh finite volume interface tracking method for surface tension dominated interfacial fluid flow. Computers & fluids, 55, 70-84.